Zoosyst. Evol. 100 (4) 2024, 1473–1486 | DOI 10.3897/zse.100.133964

PENSOFT

MUSEUM FÜR NATURKUNDE BERLIN

Evolutionary history of Chinese karst loaches (Nemacheilidae, *Karstsinnectes*): new insights from mitochondrial-based genomes and description of a new species from Guangxi, China

Tao Luo[1,2,3*], Fang-Wei Luo[1*], Chang-Ting Lan[4], Ming-Yuan Xiao[4], Jia-Jun Zhou[5], Mei Liao[1], Ning Xiao[6], Jiang Zhou[1]

1 *School of Karst Science, Guizhou Normal University, Guiyang, China*
2 *School of Life Sciences, Yunnan University, Kunming, China*
3 *Southwest United Graduate School, Kunming, China*
4 *School of Life Sciences, Guizhou Normal University, Guiyang, China*
5 *Zhejiang Forest Resource Monitoring Center, Hangzhou, China*
6 *Guiyang Healthcare Vocational University, Guiyang, China*

https://zoobank.org/326B6F9E-E524-422A-8389-570E82341BBD

Corresponding author: Jiang Zhou (zhoujiang@ioz.ac.cn)

Academic editor: Nicolas Hubert ♦ **Received** 5 August 2024 ♦ **Accepted** 10 October 2024 ♦ **Published** 5 November 2024

Abstract

The genus *Karstsinnectes* of blind fishes known as karst loaches from China was established in 2023 during a revision of the genus *Oreonectes* (Nemacheilidae). Six species are recorded in this study and some taxonomic progress has been made; however, the lack of genetic data for some species (e.g., *K. anophthalmus*) may have weakened our current understanding of *Karstsinnectes*. This study reassessed the phylogeny and evolutionary history of *Karstsinnectes* by integrating a combination of previously published and newly sequenced mitochondrial genomic data. A phylogenetic tree was developed that was able to divide *Karstsinnectes* into two clades corresponding to drainages and clarify the phylogenetic position of *K. anophthalmus*. Divergence times show that *Karstsinnectes* originated at the Oligocene/Miocene boundary (~22.37 Mya), with the most recent common ancestor occurring in the early Miocene (~18.87 Mya) and interspecific divergence occurring in the late Miocene. Ancestral area reconstruction suggests that the most recent common ancestor of *Karstsinnectes* most likely inhabited the Hongshui River basin and dispersed into the Zuojiang-Yujiang, Beipanjiang, and Youjiang river basins during the early Miocene (~18.87 Mya), middle Miocene (~12.78 Mya), and late Miocene (~6.71 Mya), respectively. The dispersal under the influence of orogenesis and a monsoon climate drove the speciation and diverse distribution of *Karstsinnectes*. Such findings are important for conservation considering that *Karstsinnectes* strictly inhabits deep caves. Additionally, the taxonomic status of the distributed *Karstsinnectes* population in Leiping Town, Daxin County, Guangxi, China was revised by combining genetic and morphological differences to describe this population as a new species, *Karstsinnectes daxinensis* Luo, Zhou & Zhou, **sp. nov.** The definition of the phylogenetic position of *K. anophthalmus* emphasizes the importance of using type locality material for the identification of cryptic species.

Key Words

Biogeography, blind fishes, *Karstsinnectes anophthalmus*, phylogeny, taxonomy

* Authors contributed equally to this work.

Copyright *Luo, T. et al.* This is an open access article distributed under the terms of the Creative Commons Attribution License (CC BY 4.0), which permits unrestricted use, distribution, and reproduction in any medium, provided the original author and source are credited.

Introduction

Southwest China features rich caves and groundwater resources, which have become the habitat of a large number of cave organisms (Duan et al. 2021; Ma et al. 2023). Chinese karst loaches in the genus *Karstsinnectes* Zhou, Luo, Wang, Zhou & Xiao, 2023 (Cypriniformes, Nemacheilidae) are a strictly troglobitic species that exhibit distinct cave-adapted characters, of which the most distinct is the unpigmented body and with eyes that are absent or highly degenerate (Lan et al. 2013; Zhu and Zhu 2014; Luo et al. 2023; Ge et al. 2024). Few people encounter the species of this genus, mainly because these species usually inhabit deep caves, have a small body size (total length < 70 mm), and have very small populations so that only two to three specimens can be collected in each survey (Lan et al. 2013; Zhu and Zhu 2014; Luo et al. 2023; Ge et al. 2024). This has indirectly contributed to the longstanding taxonomic confusion in the genus. Species of this genus were long placed within the genus *Oreonectes* Günther, 1868, until Luo et al. (2023) classified *Karstsinnectes* as a separate genus based on phylogeny. All of the species of this genus are strictly troglobitic and exhibit distinct cave-adapted characters as described above.

Although the confusing taxonomy of the genus *Karstsinnectes* has been clarified, its diversity and evolutionary history remain largely unknown. For example, the recent description of *K. cehengensis* Luo, Zhao & Zhou, 2024 and *K. longzhouensis* Ge, Du & Zhou, 2024 were based on field surveys as well as morphological and genetic data (Ge et al. 2024; Zhao et al. 2024). The discovery of these two new species may indicate that the diversity of the genus has been underestimated. Additionally, Ge et al. (2024) provided an important addition to their diagnosis and the morphology of species within the genus *Karstsinnectes* by examining additional specimens of the genus. Currently, the genus *Karstsinnectes* encompasses six recognized species that are distributed in karst caves in Guizhou Province and Guangxi Zhuang Autonomous Region, China (Fig. 1). These species include *K. acridorsalis* (Lan, 2013), *K. anophthalmus* (Zheng, 1981), *K. cehengensis*, *K. hyalinus* (Lan, Yang & Chen, 1996), *K. longzhouensis*, and *K. parvus* (Zhu & Zhu, 2014) (Zheng 1981; Lan et al. 1996, 2013; Fricke et al. 2024; Ge et al. 2024; Zhao et al. 2024). Furthermore, in several previous phylogenetic studies, samples of *K. anophthalmus* were not from the type locality (Luo et al. 2023; Ge et al. 2024; Zhao et al. 2024), and therefore, nothing is known about the true phylogenetic position of the species. In addition, despite some progress in phylogeny and classification, unknowns also exist about the origin of the genus and species of *Karstsinnectes*.

Here, to understand the phylogenetic classification and evolutionary history of the genus *Karstsinnectes*, the mitochondrial genome of Chinese karst loaches samples collected from extensive surveys over the past three years were sequenced. Specifically, the objectives of this study were to (1) infer the evolutionary relationships among species and clarify the phylogenetic position of *K. anophthalmus*; (2) identify and describe potential cryptic species; and (3) assess divergence times, reconstruct ancestral distributions, and discuss the historical biogeography of the genus *Karstsinnectes*.

Materials and methods

Taxon sampling, morphological analyses, and skeletal X-ray scanning

A total of 18 *Karstsinnectes* specimens were collected during field surveys from 2019 to 2024, from Guangxi and Guizhou in southwestern China (Fig. 1). The treatment of experimental animals in this study was consistent with the Chinese animal welfare laws (GB/T 35892–2018). All of the specimens used for morphological studies were fixed in a 10% formalin buffer and then transferred to 75% ethanol and stored at the Animal Ecology Laboratory of Guizhou Normal University (GZNU), Guiyang City, Guizhou, China. All of the molecular samples were stored at −80 °C in a refrigerator.

In total, 10 specimens of new species and *K. anophthalmus* were analyzed and measured, following Zhao et al. (2024) who measured 27 kinds of morphological data using digital calipers with an accuracy of 0.1 mm. All of the measurements were taken on the left side of each fish specimen. Morphological data were also collected from the literature for *K. acridorsalis*, *K. hyalinus*, *K. longzhouensis*, and *K. parvus* so that morphological comparisons could be made (Ge et al. 2024).

Given the morphological similarity between the new species and *K. anophthalmus*, statistical analysis was performed of the morphometric data for both species. In order to reduce the impact of allometry, a size-corrected value from the ratio of each character to standard length was calculated for the following morphometric analyses. Principal component analyses with eigenvalues greater than one, the maximum variance method, and simple bivariate scatter plots were used to explore and characterize the morphometric differences (Xu et al. 2023) between the new species and closely related species. One-way analysis of variance was conducted to determine the significance of differences in morphometric characters between the new species and the aforementioned similar species. All of the statistical analyses were performed using SPSS v.21.0 (SPSS, Inc., Chicago, IL, USA), and differences were considered statistically significant at $P < 0.05$.

Skeletal X-ray scanning was performed at the Key Laboratory of Vertebrate Evolution and Human Origins, Institute of Vertebrate Paleontology and Paleoanthropology, Chinese Academy of Sciences, using micro-computed tomography (Siemens Somatom Definition X-ray machine). The skull images were exported from a virtual 3D model which was reconstructed using Volume Graphics Studio 3.0 software.

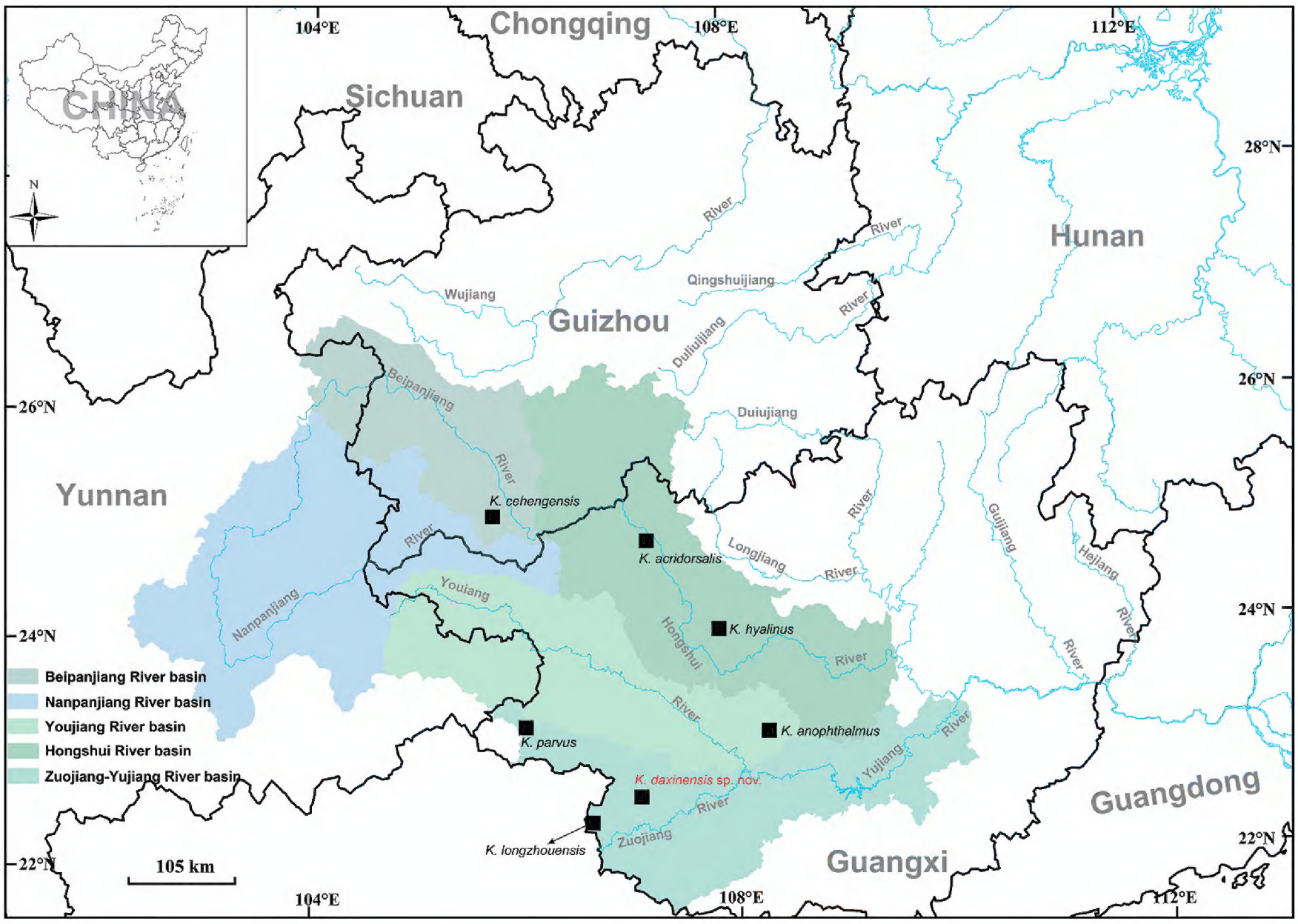

Figure 1. Geographical distribution of recognized species of the genus *Karstsinnectes* in southwestern China.

DNA extraction, sequencing, and mitogenome assembly

Total genomic DNA was extracted from three samples of three species from 95% ethanol-preserved tissues using the cetyltrimethylammonium bromide method. The process of DNA library construction and detection followed Luo et al. (2023) and DNA was sequenced by TSINGKE Biotechnology Co., Ltd. (Chengdu, Sichuan, China) on an Illumina NovaSeq 6000 platform. A total of 36 Gb of raw bases were generated, with each sample generating approximately 12 Gb of raw data. These sequencing data were completed using MitoFinder v.1.4.2 (Allio et al. 2020) for genome assembly and annotation of the mitogenome using *Oreonectes platycephalus* as the reference (accession number: NC_031579). All of the sequences have been deposited in GenBank (Table 1).

Phylogenetic construction and divergence time estimation

In this study, three mitochondrial genomes were newly sequenced while 26 mitochondrial genomes and three Cyt *b* were downloaded from the US National Center for Biotechnology Information. Two datasets were constructed for phylogenetic analysis in this study, where datasets 1 and 2 included the mitogenome and only the Cytochrome *b* (Cyt *b*), respectively. Here, the mitogenome was extracted using PhyloSuite v.1.2.3 (Zhang et al. 2020) for 13 protein coding genes, two rRNAs, and 22 tRNAs for subsequent genetic analysis.

Multiple sequence alignment was performed using MAFFT v.7.4 (Katoh and Standley 2013) within PhyloSuite v.1.2.3 (Zhang et al. 2020) and checked using MEGA v.7.0 (Kumar et al. 2016) to rule out possible errors. In addition, Partitionfinder v.2.1.1 (Lanfear et al. 2017) was used to select the best-fit partitioning and nucleotide substitution model for the two datasets, based on the Bayesian information criterion. In dataset 1, each gene fragment was pre-set as an independent partition. Luo et al. (2023) was referred to for selecting species of *Homaloptera parclitella* as an outgroup (Table 1).

Phylogenetic trees were reconstructed using Bayesian inference (BI) and maximum likelihood (ML) methods based on best-fit partitioning and nucleotide substitution models. Bayesian inference analysis was performed using MrBayes v.3.2.1 (Ronquist et al. 2012). Each BI analysis was run independently using four Markov Chain Monte Carlo chains (three heated chains and one cold chain) starting with a random tree; each chain was run for 2×10^7 generations and sampled every 1000 generations. Convergence of the data runs was confirmed when the average standard deviation of split frequencies was less than 0.01. The ML analysis was performed using IQ-tree v.2.0.4 (Nguyen et al. 2015) based on the best-fit model with 10,000 ultrafast bootstrap (UFB) replicates (Hoang et al. 2018). The ML analysis was performed until a correlation

Table 1. Localities, voucher information, and GenBank numbers for all of the samples used. NA denotes that the data is not available.

ID	Genus	Species	Localities (* type localities)	Voucher	Mitogenome
1	*Karstsinnectes*	*Karstsinnectes anophthalmus*	Xiahuang Village, Chengxiang Town, Wuming County, Guangxi, China*	WY01	PQ159188
2		*Karstsinnectes cehengensis*	Rongdu Town, Ceheng County, Guzihou, China*	GZNU 20230106003	OR936095
3		*Karstsinnectes cehengensis*	Rongdu Town, Ceheng County, Guzihou, China*	GZNU 20230106004	PP155585
4		*Karstsinnectes cehengensis*	Rongdu Town, Ceheng County, Guzihou, China*	GZNU 20230106005	PP155586
5		*Karstsinnectes cehengensis*	Rongdu Town, Ceheng County, Guzihou, China*	GZNU 20230106006	PP155587
6		*Karstsinnectes acridorsalis*	Bamu Town, Tiane County, Guangxi, China*	Tissue ID: GZNU2020	ON116515
7		*Karstsinnectes daxinensis* sp. nov.	Leiping Town, Daxin County, Guangxi, China*	GZNU 2019122201	ON116506
8		*Karstsinnectes daxinensis* sp. nov.	Leiping Town, Daxin County, Guangxi, China*	GZNU 2019011310	ON116513
9		*Karstsinnectes daxinensis* sp. nov.	Leiping Town, Daxin County, Guangxi, China*	GZNU 2019011210	ON148333
10		*Karstsinnectes daxinensis* sp. nov.	Leiping Town, Daxin County, Guangxi, China*	YJ14	PQ159190
11		*Karstsinnectes parvus*	Ande Town, Jingxi City, Guangxi, China*	Tissue ID: JTQ02	ON116520
12		*Karstsinnectes longzhouensis*	Xiadong Town, Longzhou County Guangxi, China*	LD-2023	OR947935
13		*Karstsinnectes longzhouensis*	Xiadong Town, Longzhou County Guangxi, China*	YJ18	PQ159189
14	*Oreonectes*	*Oreonectes damingshanensis*	Daming Mountain, Shanglin County, Guangxi, China*	GZNU 2020112502	ON116496
15		*Oreonectes luochengensis*	Tianhe Town, Luocheng County, Guangxi, China*	GZNU 2020011502	ON116495
16	*Micronemacheilus*	*Micronemacheilus pulcherrimus*	Duan County, Hechi City, Guangxi, China	GZNU20210609004	ON116493
17		*Micronemacheilus cruciatus*	NA	NA	AP012142
18	*Guinemachilus*	*Guinemachilus bailianensis*	Bailian cave, Liuzhou City, Guangxi, China*	GZNU 2020041603	ON116504
19		*Guinemachilus longibarbatus*	Gaoling Town, Duan County, Guangxi, China*	GZNU 2020073104	ON116508
20	*Troglonectes*	*Troglonectes microphthalmus*	Tianhe Town, Luocheng County, Guangxi, China*	GZNU 2020041601	ON116494
21		*Troglonectes shuilongensis*	Shuilong Town, Sandu County, Guizhou, China*	GZNU 2019011201	ON116522
22	*Paranemachilus*	*Paranemachilus pingguoensis*	Changping Town, Fusui County, Guangxi, China*	GZNU 2019122205	ON116500
23		*Paranemachilus genilepis*	Guohua Town, Pingguo County, Guangxi, China*	GZNU 2019122206	ON116497
24	*Yunnanilus*	*Yunnanilus jiuchiensis*	NA	NA	MW532080
25		*Yunnanilus pleurotaenia*	Fuxian Lake, Yuxi City, Yunnan Province, China	Tissue ID: GZNUCW01	ON116531
26	*Eonemachilus*	*Eonemachilus longidorsalis*	Agang Longtan pool, Luoping County, Yunnan, China	NA	NC_062728
27		*Eonemachilus niger*	NA	NA	OM681515
28	*Lefua*	*Lefua costata*	NA	NA	KT943751
29	*Traccatichthys*	*Traccatichthys zispi*	Wangxia Town, Changjiang County, Hainan, China	Tissue ID: HNMLXTQ	ON116518
30	*Triplophysa*	*Triplophysa nasobarbatula*	Dongtang Town, Libo County, Guizhou, China*	GZNU20190114001	ON116529
31	*Barbatula*	Barbatula barbatula			KP715096
32	Balitoridae	Homaloptera parclitella			AP011438

coefficient of at least 0.99 was achieved. Nodes were considered highly supported when the Bayesian posterior probability (BPP) value for the BI analysis was greater than 0.95 and the UFB value for the ML analysis was greater than 95%. Based on dataset 2, genetic distances were calculated using the uncorrected *p*-distance model and 1000 bootstrap replications, in MEGA v.7.0 (Kumar et al. 2016).

Molecular dating and time tree reconstruction was conducted in BEAST v.2.4.7 (Bouckaert et al. 2014), using dataset 1. Considering that the genus *Karstsinnectes* has no known fossil record, two calibration nodes were set up with reference to recent studies (Wang et al. 2016; Hirt et al. 2017): (1) the origin of the family Nemacheilidae dates to 45.5 million years ago (Mya) (95% confidence interval (CI): 36.7–55.8 Mya) (Hirt et al. 2017); (2) the divergence of the genera *Triplophysa* and *Barbatula* occurred at 23.5 Mya (95% CI: 20.5–26.1 Mya) (Wang et al. 2016). The BEAST analysis used an uncorrelated lognormal relaxation clock and a Yule tree prior. The BEAST analysis was run for 200 million generations and sampled every 1000 generations. All of the calibrations used a normal prior, monophyly, and standard deviation values of 2.2. Convergence of the run parameters was checked using Tracer v.1.7.1 (Rambaut et al. 2018) to ensure that the effective sample size of all of the parameters was greater than 200. Three runs were made in total, and the trees were finally merged using LogCombiner v.2.4.7. A maximum clade credibility tree was generated using TreeAnnotator v.2.4.1 (implemented in BEAST) by applying a burn-in of 25%.

Ancestral area reconstruction

Species of the genus *Karstsinnectes* are currently known to be distributed mainly in the Pearl River drainage in southern China (Fig. 1), showing a top-down distribution and can be mapped onto phylogenetic topologies (Zhao et al. 2024). To estimate the origin and dispersal of species in the genus *Karstsinnectes*, the present study conducted biogeographic analyses using the R package BioGeoBEARS (Matzke 2013). Prior to the analysis, six models were estimated using BioGeoBEARS, Dispersal-Extinction-Cladogenesis (DEC), a ML version of Dispersal-Vicariance Analysis (DIVALIKE), Bayesian biogeographical inference model (BAYAREALIKE), each with and without founder-event speciation (+J).

Results

Sequence information, phylogeny, and genetic divergence

In this study, 29 mitogenomes and three Cyt *b* sequences were collected for phylogenetic and genetic analysis. The total length of dataset 1 included 15,664 bases, 9377 conserved sites, 6263 variable sites, and 4993 parsim-informative sites. The total length of dataset 2 was 1140 bp, 871 conserved sites, 6269 variable sites, and 197 parsim-informative sites. The predefined 16 partitions of dataset 1 were suggested by Partitionfinder to be divided into five partitions and the corresponding evolutionary models were GTR+I+G, GTR+I+G, TVM+I+G, TVM+I+G, and HKY+I+G (Table 2).

Phylogenetic analyses highly supported the monophyly of *Karstsinnectes* (BPP/UFB = 1.00/100) and as the sister clade to *Guinemachilus*, *Micronemacheilus*, and *Oreonectes* (Fig. 2, Suppl. material 1). *Karstsinnectes* contains two clades (BPP/UFB = 1.00/100), where Clade I contains *K. acridorsalis* and *K. cehengensis* while Clade II contains *K. parva*, *K. longzhouensis*, *K. anophthalmus*, and a group of four samples *Karstsinnectes* sp. from Daxin County, Guangxi (Fig. 2). Divergence among species of the genus *Karstsinnectes* is highly supported (Suppl. material 1).

Table 2. Best-fit partitioning and evolutionary models used for phylogenetic analysis.

ID	Partition schemes	Length (bp)	Best Model
1	16S	1708	GTR+I+G
2	tRNAs, 12S	2523	GTR+I+G
3	ND2, ND1, ND4, ND5, ATP6, ND3, Cyt *b*	7422	TVM+I+G
4	ATP8, COI, ND4L, COIII, COII	3489	TVM+I+G
5	*ND6*	522	HKY+I+G

Genetic differences within the genus *Karstsinnectes* were assessed using Cyt *b* and ranged from 5.8 to 13.1% (Table 3). Genetic differences between samples from Daxin County, Guangxi, and species within the genus *Karstsinnectes* ranged from 6.9 (vs. *K. anophthalmus*) to 12.8% (vs. *K. acridorsalis*), with the smallest genetic distances being greater than the recognized interspecies difference of 5.8% (*K. longzhouensis* vs. *K. parvus*) (Table 3). Thus, the genetic evidence supports that the geographic population of Daxin County, Guangxi, should be treated as a new undescribed phylogenetic species.

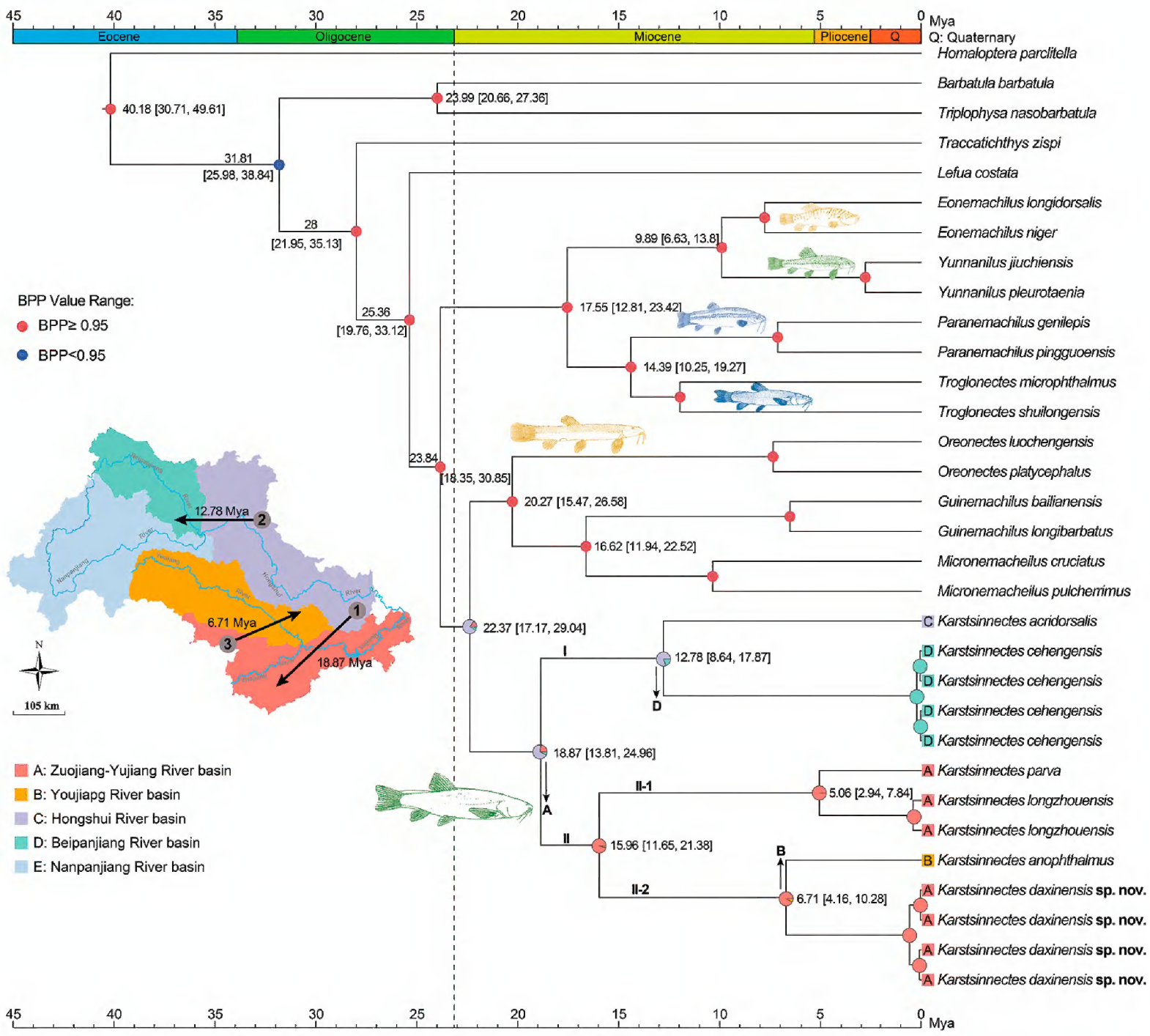

Figure 2. Chronogram and phylogeny of the genus *Karstsinnectes*. Circles at each node indicate Bayesian posterior probabilities (BPP). Colored squares at the tip of *Karstsinnectes* branches indicate species distributions, and the three major clades are marked using Roman numerals (I–II). Divergence times for major clades are marked in parentheses with 95% confidence intervals. Arrows show dispersal events. Species photos from Zhu (1989).

Table 3. Average uncorrected pairwise genetic distances (*p*-distance) among the six currently-known species of the genus *Karstsinnectes* estimated using the mitochondrial Cyt *b*.

ID	Species	1	2	3	4	5
1	*K. daxinensis* sp. nov.					
2	*K. anophthalmus*	6.9%				
3	*K. acridorsalis*	12.8%	12.1%			
4	*K. cehengensis*	10.9%	10.7%	9.4%		
5	*K. longzhouensis*	10.1%	9.6%	12.8%	11.1%	
6	*K. parvus*	10.8%	10.3%	13.1%	11.2%	5.8%

Divergence time and biogeography

The time tree in Fig. 2 shows that the genus *Karstsinnectes* originated at the Oligocene/Miocene boundary, ca. 22.37 Mya (95% CI = 17.17–29.04 Mya), with the most recent common ancestor occurring in the early Miocene, ca. 18.87 Mya (95% CI = 13.81–24.96 Mya). Interspecific divergence occurred from the middle of the Miocene to the early Pliocene (5.06–15.96 Mya), and the divergence of the Daxin population of Guangxi from its sister species *K. anophthalmus* occurred in the late Miocene, ca. 6.71 Mya (95% CI = 4.16–10.28 Mya). Additionally, the time tree provides the origins of other genera in the family Nemacheilidae. For example, the split between *Paranemachilus* and *Troglonectes* occurred ca. 14.39 Mya (95% CI = 10.25–19.27 Mya); the split between *Yunnanilus* and *Eonemachilus* occurred ca. 9.89 Mya (95% CI = 6.63–13.80 Mya); *Oreonectes* originated ca. 20.27 Mya (95% CI = 15.47–26.58 Mya); and the split between *Guinemachilus* and *Micronemacheilus* occurred between about 16.62 Mya (95% CI = 11.94–22.52 Mya) (Fig. 2).

The results of model comparisons used for ancestral area reconstruction within BioGeoBEARS are provided in Table 4. Based on the DEC+J model (Fig. 2, Suppl. material 2, 3), dispersal events may have shaped the current distribution of *Karstsinnectes*. Biogeographical inference based on the best model, DEC+J (AIC weight = 0.53; Table 4), suggests that the most recent common ancestor of extant *Karstsinnectes* likely inhabited the Hongshui River basin and then dispersed southwestward into the Zuojiang-Yujiang and Beipanjiang river basins (Fig. 2). After colonizing the Zuojiang-Yujiang River basin, the genus dispersed eastward into the Youjiang River basin. The BAYAREALIKE+J model (AIC weight = 0.47; Table 4; Suppl. material 4) was second-best and yielded similar results.

Morphological differences

Principal component analysis of the new species and *K. anophthalmus* using 18 measured characters showed that a total of five principal component (PC) factors were extracted based on eigenvalues greater than one. The first three components explained 69.45% of the total variance, with PC1 accounting for 37.97%, PC2 for 17.75%, and PC3 for 13.74% (Table 5). In the scatterplot of PC1 versus PC2, *K. daxinensis* sp. nov. and *K. anophthalmus* formed distinct clusters that were separated on the PC1 axis (Fig. 3). Body depth, caudal peduncle depth, head depth, head width, mouth width, and maxillary barbel length were mainly loading on PC1 (Table 5). Analysis of variance indicated that 40% of the 20 morphometric characters shared by *K. daxinensis* sp. nov. and *K. anophthalmus* were significantly different (Table 6). When compared with *K. anophthalmus*, *K. daxinensis* sp. nov. has a smaller predorsal length (15.1 ± 2.0 vs. 18.9 ± 2.6), prepelvic length (13.8 ± 1.2 vs. 18.1 ± 2.7), head length (5.4 ± 0.5 vs. 7.3 ± 0.9), head depth (2.1 ± 0.4 vs. 3.1 ± 0.5), head width (3.4 ± 0.7 vs. 4.8 ± 0.8), mouth width (1.7 ± 0.2 vs. 2.7 ± 0.4), but for inrostral barbel length, *K. daxinensis* sp. nov. is larger than *K. anophthalmus* (2.2 ± 0.5 vs. 1.3 ± 0.1) (Table 6).

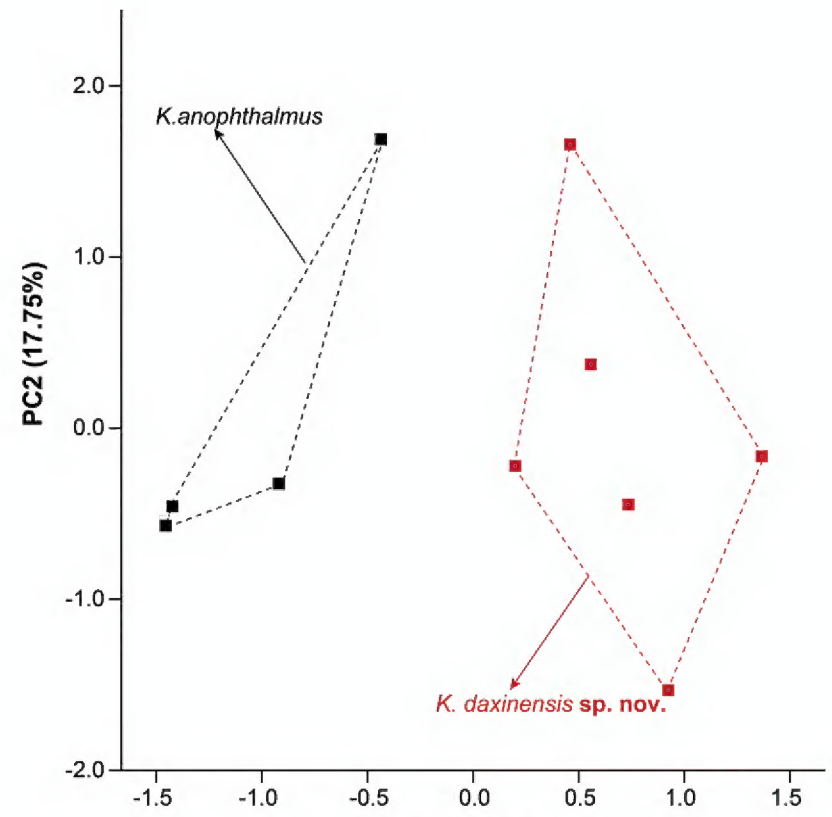

Figure 3. Scatter plots of the 1st and 2nd principal components for *Karstsinnectes daxinensis* sp. nov. and *K. anophthalmus*.

Table 4. Estimated and statistical results for six models (DEC, DIVALIKE, BAYAREALIKE, and their corresponding +J models) using the R package BioGeoBEARS. The model with the maximum AIC model weight is the best model and is indicated using bold. Abbreviations: LnL referred to log-likelihood; *d*, rate of dispersal; *e*, rate of extinction; *j*, likelihood of founder-event speciation at cladogenesis; AIC, Akaike's information criterion.

Model	LnL	Number of parameters	*d*	*e*	*j*	AIC	AIC model weight
DEC	-72.37	2	4.50E-03	9.90E-03	0	148.7	4.00E-10
DEC+J	**-50.37**	**3**	**1.00E-12**	**1.00E-12**	**0.042**	**106.7**	**0.53**
DIVALIKE	-63.76	2	0.0039	1.00E-12	0	131.5	2.20E-06
DIVALIKE+J	-63.76	2	0.0039	1.00E-12	0	131.5	2.20E-06
BAYAREALIKE	-82.37	2	8.10E-03	4.70E-02	0	168.7	1.80E-14
BAYAREALIKE+J	-50.48	3	1.00E-07	1.00E-07	0.041	107	0.47

Table 5. PCA loadings of the five principal components extracted from 18 measured characters of morphometric data for *Karstsinnectes daxinensis* sp. nov. and *K. anophthalmus*.

	PC1	PC2	PC3	PC4	PC5
Standard length	-0.182	-0.865	0.145	0.322	-0.087
Body depth	-0.849	-0.311	-0.061	-0.039	-0.257
Predorsal length	-0.014	0.293	-0.104	0.502	0.699
Dorsal fin length	-0.198	-0.264	0.128	-0.676	0.593
Preanal length	0.447	0.310	-0.706	-0.126	0.303
Analfin length	0.518	0.735	0.157	-0.228	-0.325
Pectoral fin length	0.356	0.443	0.689	-0.100	0.112
Prepelvic length	-0.574	0.665	-0.290	-0.269	-0.219
Pelvic fin length	0.530	-0.137	-0.405	-0.047	-0.371
Caudal peduncle length	0.066	0.299	0.778	-0.330	0.072
Caudal peduncle depth	0.737	-0.079	-0.316	0.293	0.332
Head length	-0.552	0.731	-0.283	0.177	0.130
Head depth	-0.781	0.318	0.241	0.461	-0.031
Head width	-0.711	0.076	0.263	0.440	-0.084
Mouth width	-0.920	0.268	-0.101	0.180	0.103
Outrostral barbel length	0.711	0.002	0.495	0.446	0.141
Inrostral barbel length	0.767	0.295	-0.063	0.412	-0.387
Maxillary barbel length	0.963	0.075	0.041	0.092	-0.014
Eigenvalues	0.314	2.854	0.608	1.51	0.71
Percentage of total variance	37.967	17.746	13.736	11.163	9.058
Cumulative percentage	37.967	55.714	69.449	80.612	89.670

Taxonomic account

***Karstsinnectes daxinensis* Luo, Zhou & Zhou, sp. nov.**

https://zoobank.org/BA75B4CD-0B3E-4EC6-AD2A-CB8556244BA7

Suppl. material 5, Figs 4, 5

Chresonymy. *Oreonectes anophthalmus*: Wang, 2022 (Leiping Town, Daxin County, Guangxi, China). *Karstsinnectes anophthalmus*: Luo et al. 2023, 2024; Yu et al. 2023; Ge et al. 2024; Zhao et al. 2024 (Leiping Town, Daxin County, Guangxi, China).

Holotype. GZNU20200427002, 30.8 mm total length, 27.5 mm standard length (SL), collected by Tao Luo on April 27, 2020, in Leiping Town, Daxin County, Chongzuo City, Guangxi Zhuang Autonomous Region, China (22.64141996°N, 107.1030802°E; ca. 155 m a.s.l.).

Paratypes. Five specimens from the same locality as the holotype: GZNU20200427001, GZNU20200427006, GZNU20200427003–427005, collected by Tao Luo on April 27, 2020.

Etymology. The specific epithet "*daxinensis*" refers to the type locality of the new species: Leiping Town, Daxin County, Chongzuo City, Guangxi, China. We propose the English common name "Daxin Chinese Karst Loach" and Chinese common name "Dà Xīn Zhōng Huá Kā Qiū (大新中华喀鳅)."

Diagnosis. *Karstsinnectes daxinensis* sp. nov. can be distinguished from all of the other congeners by the following combination of characters: (1) body naked and without pigmentation; (2) eyes absent; (3) dorsal-fin rays iii-7, pectoral-fin rays i-10–11, pelvic-fin rays i-5, anal-fin rays iii-5, caudal fin truncated with 13–14 branched caudal-fin rays; (4) pelvic fins slightly long, length 9.5–13.2% of SL, tip reaching the anus; (5) high and wide head (depth 6.3–9.8% of SL; wide 10.0–14.8% of SL), narrow mouth (width 6.2–7.9% of SL), long inrostral barbel length (length 7.2–12.7% of SL), and long maxillary barbel length (length 11.3–13.1% of SL).

Description. Morphological data of all of the specimens of *Karstsinnectes daxinensis* sp. nov. were collected in this study are provided in Table 6 and Suppl. material 5.

Body elongated and cylindrical, anterior portion gradually raised from upper eye to dorsal-fin base, posterior portion gradually compressed from dorsal fin to caudal-fin base, with deepest body depth anterior to dorsal-fin origin, deepest body depth 9.1–10.4% of SL. Dorsal profile of forehead and predorsal profile convex, concave from dorsal-fin origin to anterior margin of upper caudal adipose keel. Ventral profile flat. Head short, length 18.9–23.6% of SL, slightly depressed and flattened, width greater than depth (head depth/head length = 29.2–42.6%). Snout short and lightly blunt. Mouth inferior, snout tip truncated, upper and lower lips smooth, lower lip with a V-shaped median notch.

Three pairs of barbels: inrostral barbels short, length 7.2–12.7% of SL, tip not reaching to corner of the mouth; outrostral barbel long, length 9.4–12.7% of SL, tip reaching to posterior margin of the eye. Maxillary barbel slightly developed, length 11.3–13.1% of SL, tip not reaching to anterior margin of operculum. Anterior and posterior nostrils adjacent. Anterior nostril tube long, truncated, without elongated long barbel-like tip. Eyes absent. Gill rakers not developed, 9–10 gill rakers on first gill arch ($n = 2$).

Dorsal-fin rays iii-7, pectoral-fin rays i-10–11, pelvic-fin rays i-5, anal-fin rays iii-5, and with 13–14 branched caudal-fin rays. Dorsal fin short, length 12.7–17.2% of SL, distally margin truncated, origin slightly posterior to pelvic-fin insertion, first branched ray longest, tip of dorsal fin slight beyond to vertical of anus. Pectoral fin slightly developed, length 12.8–14.8% of SL, tip not beyond midpoint between origins of pectoral and pelvic fins. Pelvic fin slightly long, length 9.5–13.2% of SL, distally margin oval, vertically aligned with first unbranched ray of dorsal fin, tip of pelvic fin reaching the anus. Anal fin slightly long, length 11.7–16.8% of SL, tip not reaching to caudal-fin base. Caudal fin truncated, upper lobe is equal in length to lower one, tip pointed, caudal peduncle length 13.2–16.8% of SL, caudal peduncle depth 7.4–10.4% of body depth, with not developed adipose crests along both dorsal and ventral sides. Total vertebrae: 4 + 31 ($n = 1$) (Fig. 4D).

Body naked, smooth, and scaleless. Cephalic lateral line system developed. Lateral line and head sensory pores absent. Two chambers of air-bladder, anterior chamber dumbbell-shaped and membranous, open on both sides and posteriorly (Fig. 4E), and posterior chamber slight developed, slightly filling body cavity, connected with anterior chamber by short tube.

Coloration. In cave water bodies when living, body semi-translucent and pale pink, without skin pigment, and all of the fins hyaline (Fig. 5). After fixation in 7% formalin solution, the body color was yellowish white, thorax and gills light brown color, transparent on all of the fins (Fig. 4A–C).

Table 6. Morphometric statistics and results of analysis of variance from *Karstsinnectes daxinensis* sp. nov. and *K. anophthalmus*. Abbreviations: *Kd*, *K. daxinensis* sp. nov.; *Ka*, *K. anophthalmus*. NA denotes that the data is not available.

	***K. daxinensis* sp. nov. (n = 6)**		***K. anophthalmus* (n = 4)**		***P*-value from ANOVA**
	Range	**Mean ± SD**	**Range**	**Mean ± SD**	***Kd* vs. *Ka***
Total length	26.4–32.3	29.1 ± 2.9	30.5–42.8	36.5 ± 5.1	0.055
Standard length	22.1–27.8	25.0 ± 2.8	25.3–36.9	31.4 ± 4.8	0.055
Body depth	2.4–3.2	2.9 ± 0.4	2.8–5.3	4.2 ± 1.1	0.054
Body width	1.9–2.9	2.3 ± 0.5	NA	NA	NA
Predorsal length	12.6–17.9	15.1 ± 2.0	15.8–22.0	18.9 ± 2.6	0.033
Dorsal fin base length	1.8–2.6	2.3 ± 0.3	NA	NA	NA
Dorsal fin length	2.9–4.6	3.9 ± 0.7	4.1–6.0	5.3 ± 0.8	0.055
Preanal length	16.8–20.3	18.8 ± 1.6	19.3–25.1	23.0 ± 2.6	0.055
Anal fin base length	1.3–1.9	1.6 ± 0.2	NA	NA	NA
Anal fin length	2.7–3.7	3.3 ± 0.4	3.5–4.2	3.7 ± 0.3	0.240
Prepectoral length	4.1–5.7	4.8 ± 0.7	NA	NA	NA
Pectoral fin base length	0.7–1.4	1.0 ± 0.3	NA	NA	NA
Pectoral fin length	2.9–4.1	3.5 ± 0.6	3.9–4.8	4.3 ± 0.4	0.055
Prepelvic length	12.3–15.0	13.8 ± 1.2	14.8–21.2	18.1 ± 2.7	0.033
Pelvic fin base length	0.6–0.9	0.8 ± 0.1	NA	NA	NA
Pelvic fin length	2.3–3.0	2.7 ± 0.3	1.4–3.0	2.6 ± 0.8	0.285
Caudal peduncle length	3.0–4.6	3.8 ± 0.7	4.1–6.3	4.8 ± 1.0	0.136
Caudal peduncle depth	1.6–2.4	2.2 ± 0.3	1.7–2.7	2.1 ± 0.4	0.670
Head length	4.8–6.0	5.4 ± 0.5	6.2–8.4	7.3 ± 0.9	0.011
Head depth	1.4–2.5	2.1 ± 0.4	2.6–3.7	3.1 ± 0.5	0.010
Head width	2.2–4.0	3.4 ± 0.7	3.7–5.5	4.8 ± 0.8	0.033
Upper jaw length	0.9–1.5	1.2 ± 0.2	NA	NA	NA
Lower jaw length	0.8–1.1	1.0 ± 0.1	NA	NA	NA
Mouth width	1.4–1.9	1.7 ± 0.2	2.2–3.2	2.7 ± 0.4	0.011
Outrostral barbel length	2.1–3.5	2.8 ± 0.6	2.1–3.1	2.6 ± 0.4	0.394
Inrostral barbel length	1.6–2.8	2.2 ± 0.5	1.1–1.3	1.3 ± 0.1	0.011
Maxillary barbel length	2.6–3.6	3.1 ± 0.4	2.3–2.6	2.5 ± 0.1	0.087

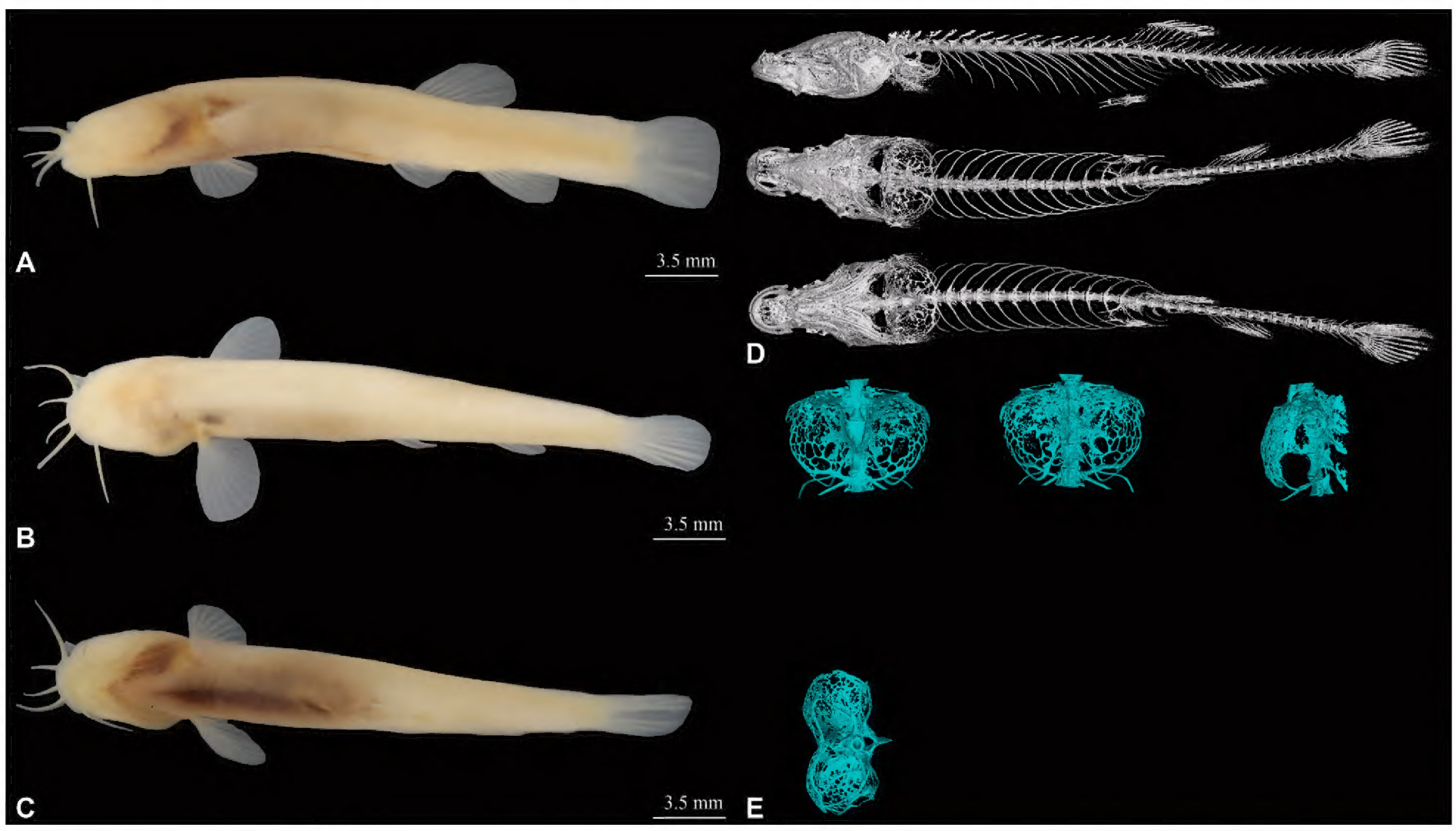

Figure 4. *Karstsinnectes daxinensis* sp. nov., GZNU20200427002, holotype, 27.5 mm standard length; Zuojiang River basin, Leiping Town, Daxin County, Guangxi, China. **A**. Lateral view; **B**. Dorsal view; **C**. Ventral view; **D**. Micro-computed tomography of lateral, dorsal, and ventral views of body; **E**. Ventral, dorsal, lateral, and from above views of air bladder posterior chamber based on micro-computed tomography.

Comparisons. Morphological data of *K. daxinensis* sp. nov. with the six known species within genus *Karstsinnectes* are given in Table 7.

Karstsinnectes daxinensis sp. nov. can be distinguished from *K. cehengensis*, *K. acridorsalis*, *K. parvus*, *K. hyalinus*, and *K. longzhouensis* by caudal fin truncated

Table 7. Comparison of the diagnostic characters of the new species described here, *Karstsinnectes daxinensis* sp. nov., with those selected for the six other known species of the genus *Karstsinnectes*. Modified from Zhao et al. (2024). Abbreviations: *K. an*, *K. anophthalmus*; *K. ce*, *K. cehengensis*; *K. ac*, *K. acridorsalis*; *K. pa*, *K. parvus*; *K. hy*, *K. hyalinus*; and *K. lo*, *K. longzhouensis*.

	***K. daxinensis* sp. nov.**	***K. an***	***K. ce***	***K.ac***	***K. pa***	***K. hy***	***K. lo***
Caudal fin	Truncated	Truncated	Forked	Forked	Forked	Forked	Forked
Eyes	Absent	Absent	Reduced	Absent	Absent	Absent	Absent
Scales	Absent	Absent	Absent	Absent	Absent	Present (tiny scales)	Absent
Lateral line	Absent	Absent	Incomplete	Absent	Present	Absent	Present
Dorsal-fin rays	iii, 7	iii, 7	iii, 7	iii, 8–9	iii, 9	ii, 9	iii, 9
Anal-fin rays	iii, 5	ii, 5	iii, 5	ii, 5	iii, 5	ii, 4	iii, 5
Pectoral-fin rays	i, 10–11	i, 10–12	ii, 11–12	i, 10	i, 10	i, 11	i, 10/12
Pelvic-fin rays	i, 5	i, 4–5	i, 7	i, 5	i, 6	i, 5	i, 5
Caudal-fin rays	13–14	12–13	14	13–14	12–13	11–12	13–14
Gill rakers	9–10	8–9	9	9	11	12	11–12
Dorsal-fin rays tip	Slightly beyond to anal-fin insertion	Far beyond to anal-fin insertion	Reaching to anal-fin insertion	Far beyond to anal-fin insertion	Far beyond to anal-fin insertion	Reaching to anal-fin insertion	Far beyond to anal-fin insertion
Dorsal fin origin	Slightly posterior to pelvic-fin origin	Posterior to pelvic-fin origin	Slightly posterior to pelvic-fin origin	Posterior to pelvic-fin origin	Anterior to pelvic-fin origin	Slightly anterior to pelvic-fin origin	Anterior to pelvic-fin origin
Pelvic fin tip	Reaching the anus	Not reaching the anus	Not reaching the anus	Not reaching the anus	Exceeding anus	Reaching the anus	Reaching the anus
Distribution	Zuojiang River	Youjiang River	Beipanjiang River	Hongshui River	Youjiang River	Hongshui River	Zuojiang River
Source	This study	Lan et al. 2013	Zhao et al. 2024	Lan et al. 2013; Ge et al. 2024	Zhu and Zhu, 2014; Ge et al. 2024	Lan et al. 1996; Ge et al. 2024	Ge et al. 2024

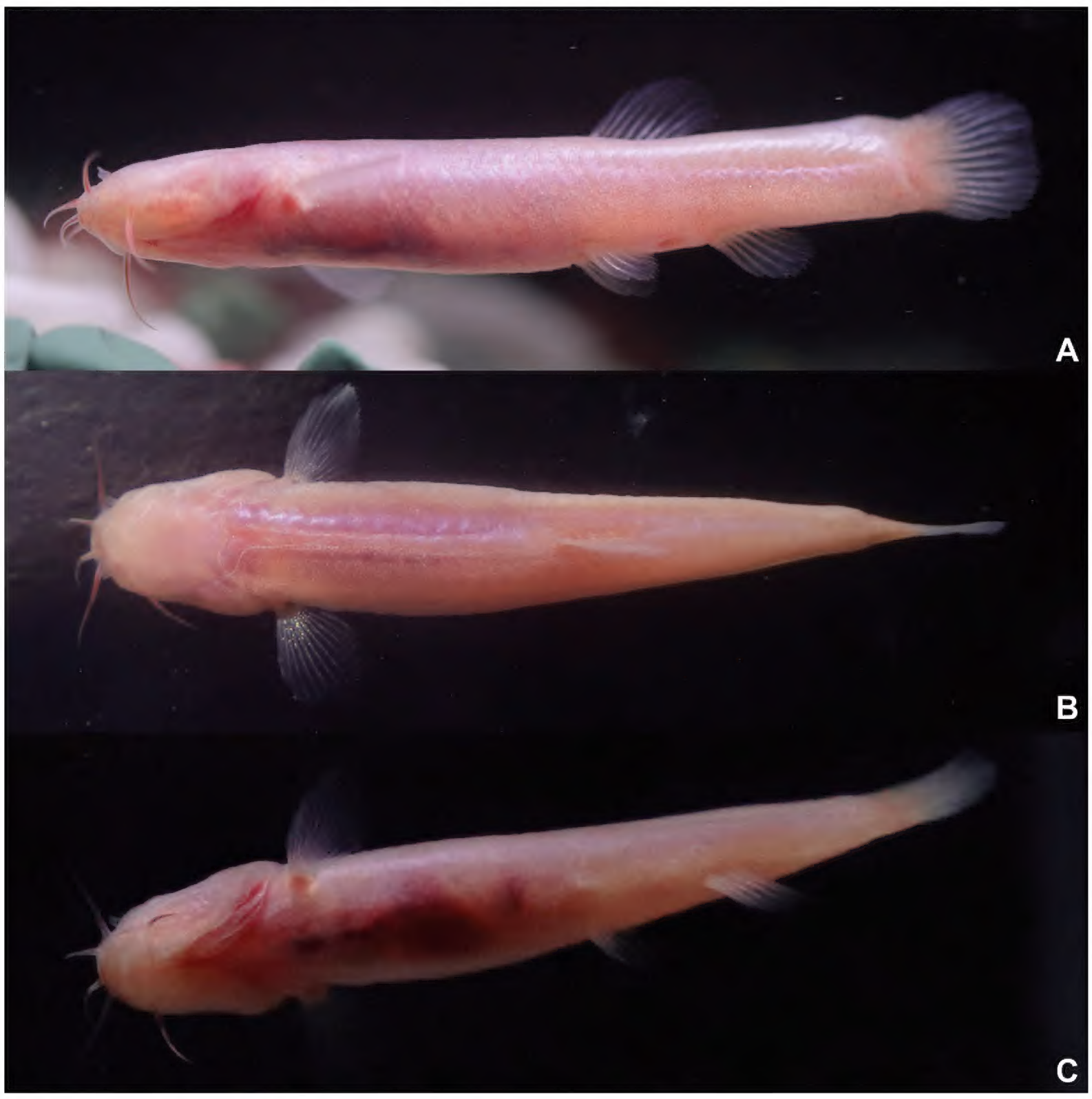

Figure 5. Lateral, dorsal, ventral views of *Karstsinnectes daxinensis* sp. nov. In living.

(vs. forked). The new species can be further distinguished from *K. cehengensis* by eye absent (vs. reduced); and from *K. cehengensis*, *K. parvus*, and *K. longzhouensis* by lateral line absent (vs. present).

Morphologically and genetically, *K. daxinensis* sp. nov. is closest to *K. anophthalmus*, but can still be distinguished by some morphological characters. *Karstsinnectes daxinensis* sp. nov. different from *K. anophthalmus* by tip of pelvic fin reaching the anus (vs. not reaching the anus) (Fig. 6), three unbranched pelvic-fin rays (vs. two), narrow mouth (6.2–7.9% of SL vs. 8.7–8.8% of SL), long inrostral barbel length (7.2–12.7% of SL vs. 3.4–5.3% of SL), and long maxillary barbel length (11.3–13.1% of SL vs. 7.1–10.0% of SL).

Distribution. At present, this new species *K. daxinensis* sp. nov. has only been discovered in the type locality and nearby caves within the Zuojiang River basin (Fig. 1).

Discussion

The genus *Karstsinnectes*, a group of truly blind fishes, has only six species which have all been described in the last 40 years, indicating that the genus has a low level of species diversity which may be a result of the lack of thorough field surveys. We have comprehensively reconstructed the phylogenetic and evolutionary history of *Karstsinnectes* for the first time by integrating the mitochondrial genome. Phylogenic analysis revealed that *Karstsinnectes* can be divided into two clades and follows an intriguing pattern in which phylogeny corresponds to geographical distribution. The divergence time and ancestral area reconstruction suggest that the genus *Karstsinnectes* originated at the Oligocene/Miocene boundary at ~22.37 Mya (~17.17–29.04 Mya), with the most recent common ancestor found

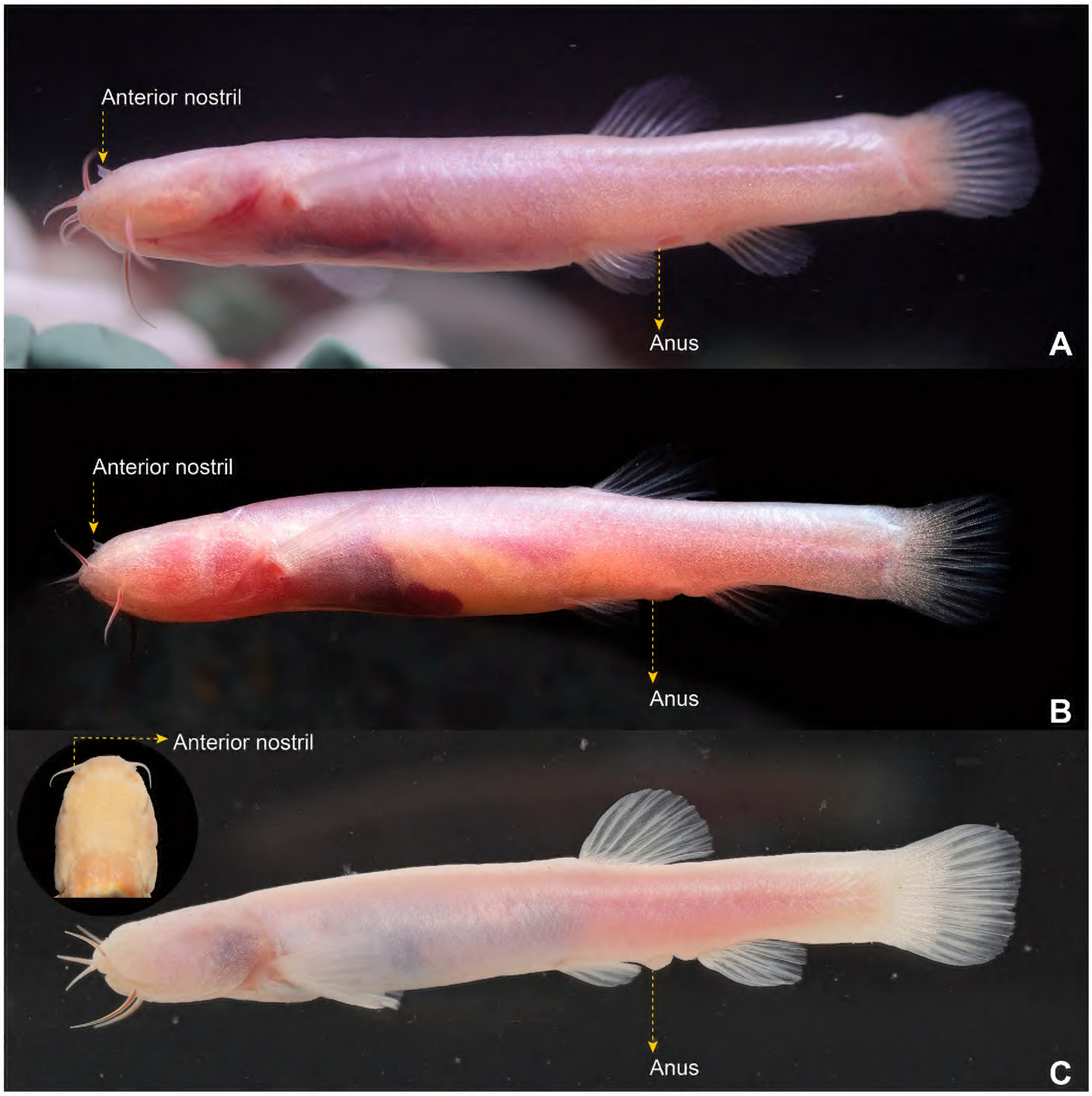

Figure 6. Morphological comparison of *Karstsinnectes daxinensis* sp. nov. (**A**) and *K. anophthalmus* (**B, C**). This mainly shows the relative locations at the tip of the pelvic fin and the anus separating these two species. Photo **A** by Tao Luo, Photos **B, C** by Mr. Jia-Jun Zhou and Mr. Jia-Hu Lan.

to occur ~18.87 Mya, and that dispersal events have shaped the current distribution pattern of diversity in the genus *Karstsinnectes*.

Paleogeoclimatic events and the formation of karst landscapes drove the origin and dispersal of *Karstsinnectes*. Dispersal played an important role within the evolution of *Karstsinnectes*. Ancestral area reconstruction results suggest that the most recent common ancestor of *Karstsinnectes* species most likely inhabited the Hongshui River basin, then dispersed to the Zuojiang-Yujiang (18.87 Mya) and Beipanjiang (~12.78 Mya) river basins. At ~6.71 Mya, the ancestor of Clade II-2 dispersed to the Youjiang River basin from the Zuojiang-Yujiang River basin. These dispersal events suggest that the formation of the modern conditions between the Beipanjiang and Hongshui rivers, between the Hongshui and Zuojiang-Yujiang rivers, and between the basins of the Zuojiang-Yujiang and Youjiang rivers dates back to at least the middle to late Miocene (~6.71–18.87 Mya). Notably, these basins are situated on the right side of the Ailao Shan-Red River shear zone. Geological and phylogenetic evidence has shown that at least two rapid orogenic events occurred in the Ailao Shan-Red River shear zone, first during the late Eocene-early Miocene (16–35 Mya) and second in the late Miocene (5–11 Ma) (Leloup et al. 2001; Gilley et al. 2003; Li et al. 2024). Geological evidence also suggests that several accelerations of uplift of the Qinghai-Xizang Plateau occurred (An et al. 2006), with the most dramatic one occurring at 15–25 Mya (Ding et al. 2017, 2022). Additionally, the uplift of the Qinghai-Xizang Plateau caused a rapid shift in the climate of East Asia to a monsoon-dominated pattern (Wu et al. 2022); the large amounts of rainfall brought about by intensification of the monsoon (Farnsworth et al. 2019) provided an additional impetus for the dispersal and speciation of *Karstsinnectes*. As a result of these paleogeoclimatic events, during the Miocene, the landforms of southwestern China were reorganized above and below ground, including high mountains, valleys, rivers, and caves (He et al. 2023; Lu et al. 2023). During the same period, dramatic orogeny and rainfall also accelerated the formation of karst caves and upstream drainage systems of the Pearl River (Che and Yu 1985; Zhang et al. 2023), e.g., the Beipanjiang, Hongshui, Zuojiang, and Youjiang rivers, which is consistent with palaeogeological evidence (Zhang et al. 2023). Subterranean caves and rivers generated by paleogeoclimatic events created ecological conditions that allowed for the dispersal and formation of cave fishes. Together, these appear to be consistent with our estimates of divergence times based on DNA data and with spatial and temporal changes in the diversification of other cave-dwelling fishes (Wen et al. 2022), suggesting the possibility that orogeny, cave formation, and monsoon winds have played a role in facilitating the formation and dispersal of cave species.

The diversity of *Karstsinnectes* needs to be further assessed using a combination of field surveys along with genetic and morphological analysis. Based on morphological characters, specimens of *Karstsinnectes* from Daxin, Guangxi, were previously treated as *K. anophthalmus* (Luo et al. 2023; Yu et al. 2023; Ge et al. 2024; Zhao et al. 2024), but were not compared with *K. anophthalmus* from the type locality. Previous studies have noted morphological differences between the Daxin population and *K. anophthalmus*, but lacked data to support separating them taxonomically (Ge et al. 2024). Genetically, the genetic distance between the new species and *K. anophthalmus* from the type locality was 6.9%, which was greater than that between other species of the same genus, e.g., *K. longzhouensis* and *K. parvus* had a genetic distance of 5.8% (Table 3), genetically supporting the validity of the new species. *Karstsinnectes daxinensis* sp. nov. and *K. anophthalmus*are also morphologically distinguishable (see Comparisons). This work has emphasized that the use of type locality data is very important for the correct identification of cryptic species. Additionally, the longer branch lengths, the older divergence times, and the discontinuity in distribution suggest that there may be undiscovered populations, e.g., only *K. anophthalmus* occurs in the Youjiang River basin (Fig. 1), which needs to be further explored with new field surveys.

Key to species of *Karstsinnectes*, from southwest China (modified from Zhao et al. 2024; Ge et al. 2024).

1	Eyes reduced, two unbranched pectoral-fin rays	*K. cehengensis*
–	Eyes absent, single unbranched pectoral-fin rays	2
2	Caudal fin truncated	3
–	Caudal fin forked	4
3	Three unbranched anal-fin rays, tip of pelvic fin reaching the anus	*Karstsinnectes daxinensis* sp. nov.
–	Two unbranched anal-fin rays, tip of pelvic fin not reaching the anus	*K. anophthalmus*
4	Body covered by tiny scales	*K. hyalinus*
–	Body scaleless	5
5	Lateral line absent	*K. acridorsalis*
–	Lateral line absent	6
6	Pectoral fin with 10 branched rays, five branched pelvic fin rays	*K. parvus*
–	Pectoral fin with 11 or 12 branched rays, six branched pelvic fin rays	*K. longzhouensis*

Acknowledgments

We thank Jing Yu, Ya-Li Wang, and Xu Yang for their help during the sample collection. We thank Prof. Li-Na Du and Mr. Jia-Hu Lan for providing the morphometric data and photos of *K. anophthalmus*. We thank Dr. Jing-Song Shi for his help with the CT scan of the bones. Finally, we thank LetPub (www.letpub.com.cn) for its linguistic assistance during the preparation of this manuscript. This study was supported by the programs of the Diversity and Distribution Survey of Chiroptera species in China (2021FY100302), the Guizhou Province Top Discipline Construction Program Project (Qianjiao Keyan Fa [2019] 125), and the Guizhou Normal University Academic Emerging Talent Fund Project (Qianshi Xin Miao [2021]).

References

Allio R, Schomaker-Bastos A, Romiguier J, Prosdocimi F, Nabholz B, Delsuc F (2020) MitoFinder: Efficient automated large-scale extraction of mitogenomic data in target enrichment phylogenomics. Molecular Ecology Resources 20(4): 892–905. https://doi.org/10.1111/1755-0998.13160

An Z, Zhang P, Wang E, Wang S, Qiang X, Li L, Song Y, Chang H, Liu X, Zhou W, Liu W, Cao J, Li X, Shen J, Liu Y, Ai L (2006) Changes of the monsoon-arid environment in China and growth of the Tibetan Plateau since the Miocene. Quaternary Sciences 26(5): 678–693.

Bouckaert R, Heled J, Kühnert D, Vaughan T, Wu C-H, Xie D, Suchard MA, Rambaut A, Drummond AJ (2014) BEAST 2: A Software Platform for Bayesian Evolutionary Analysis. PLoS Computational Biology 10(4): e1003537. https://doi.org/10.1371/journal.pcbi.1003537

Che YT, Yu JZ (1985) Karst in China. Beijing: Science Press, 88–95. [in Chinese]

Ding L, Spicer RA, Yang J, Xu Q, Cai F, Li S, Lai Q, Wang H, Spicer TEV, Yue Y, Shukla A, Srivastava G, Khan MA, Bera S, Mehrotra R (2017) Quantifying the rise of the Himalaya orogen and implications for the South Asian monsoon. Geology 45(3): 215–218. https://doi.org/10.1130/G38583.1

Ding L, Kapp P, Cai F, Garzione CN, Xiong Z, Wang H, Wang C (2022) Timing and mechanisms of Tibetan Plateau uplift. Nature Reviews Earth & Environment 3(10): 652–667. https://doi.org/10.1038/s43017-022-00318-4

Duan YF, Li M, Xu KW, Zhang L, Zhang LB (2021) Protect China's karst cave habitats. Science 374(6568): 699–699. https://doi.org/10.1126/science.abm5389

Farnsworth A, Lunt DJ, Robinson SA, Valdes PJ, Roberts WH, Clift PD, Markwick P, Su T, Wrobel N, Pancost RD (2019) Past East Asian monsoon evolution controlled by paleogeography, not CO_2. Science Advances 5(10): eaax1697. https://doi.org/10.1126/sciadv.aax1697

Fricke R, Eschmeyer WN, Van der Laan R (eds) (2024) Catalog of fishes: genera, species, references. California Academy of Sciences, San Francisco. http://researcharchive.calacademy.org/research/ichthyology/catalog/fishcatmain.asp. [Electronic version accessed 8 August 2024]

Ge JY, Nong ZQ, Yang J, Du LN, Zhou JJ (2024) Taxonomic revision of the cavefish genus *Karstsinnectes* (Cypriniformes, Nemacheilidae), with a description of a new species from Guangxi Province, China. Zoosystematics and Evolution 100(2): 663–673. https://doi.org/10.3897/zse.100.118061

Gilley LD, Harrison TM, Leloup PH, Ryerson FJ, Lovera OM, Wang JH (2003) Direct dating of left-lateral deformation along the Red River shear zone, China and Vietnam. Journal of Geophysical Research: Solid Earth 108(B2): 2127. https://doi.org/10.1029/2001JB001726

Günther A (1868) Catalogue of the fishes in the British museum. Trustees of the British Museum, London.

He J, Garzanti E, Jiang T, Barbarano M, Liu E, Chen S, Liao Y, Li X, Wang H (2023). Evolution of eastern Asia river systems reconstructed by the mineralogy and detrital-zircon geochronology of modern Red River and coastal Vietnam river sand. Earth-Science Reviews 245: 104572. https://doi.org/10.1016/j.earscirev.2023.104572

Hirt MV, Arratia G, Chen WJ, Mayden RL, Tang KL, Wood RM, Simons AM (2017) Effects of gene choice, base composition and rate heterogeneity on inference and estimates of divergence times in cypriniform fishes. Biological Journal of the Linnean Society 121(2): 319–339. https://doi.org/10.1093/biolinnean/blw045

Hoang DT, Chernomor O, von Haeseler A, Minh BQ, Vinh LS (2018) UFBoot2: Improving the ultrafast bootstrap approximation. Molecular Biology and Evolution 35(2): 518–522. https://doi.org/10.1093/molbev/msx281

Katoh K, Standley D M (2013) MAFFT multiple sequence alignment software version 7: improvements in performance and usability. Molecular Biology and Evolution 30(4): 772–780. https://doi.org/10.1093/molbev/mst010

Kumar S, Stecher G, Tamura K (2016) MEGA7: Molecular evolutionary genetics analysis version 7.0 for bigger datasets. Molecular Biology and Evolution 33(7): 1870–1874. https://doi.org/10.1093/molbev/msw054

Lan JH, Yang JX, Chen YR (1996) One new species of cavefish from Guangxi (Cypriniformes: Cobitidae). Zoological Research 17(2): 109–112.

Lan JH, Gan X, Wu TJ, Yang J (2013) Cave Fishes of Guangxi, China. Beijing: Science Press, 68–98. [in Chinese]

Lanfear R, Frandsen PB, Wright AM, Senfeld T, Calcott B (2017) PartitionFinder 2: New methods for selecting partitioned models of evolution for molecular and morphological phylogenetic analyses. Molecular Biology and Evolution 34(3): 772–773. https://doi.org/10.1093/molbev/msw260

Leloup PH, Arnaud N, Lacassin R, Kienast JR, Harrison TM, Trong TP, Replumaz A, Tapponnier, P (2001) New constraints on the structure, thermochronology, and timing of the Ailao Shan-Red River shear zone, SE Asia. Journal of Geophysical Research: Solid Earth 106(B4): 6683–6732. https://doi.org/10.1029/2000JB900322

Li XQ, Peng HW, Xiang KL, Xiang XG, Jabbour F, Ortiz RDC, Soltis PS, Wang W (2024) Phylogenetic evidence clarifies the history of the extrusion of Indochina. Proceedings of the National Academy of Sciences of the United States of America 121(35): e2322527121. https://doi.org/10.1073/pnas.2322527121

Lu H, Feng H, Lyu H, Wang H, Zhang X, Zhang H, Wang X, Li Y (2023) Formation and evolution of the Asian landscape during the Cenozoic. The Innovation Geoscience 1(2): 100020. https://doi.org/10.59717/j.xinn-geo.2023.100020

Luo T, Yang Q, Wu L, Wang YL, Zhou JJ, Deng HQ, Xiao N, Zhou J (2023) Phylogenetic relationships of cavefishes of the Nemacheilidae (*Heminoemacheilus*, *Oreonectes*, *Yunnanilus*, *Paranemachilus*,

and *Troglonectes*) revealed by phylogenetic analysis of mitochondrial genome and seven nuclear genes. Zoological Research 44(4): 693–697. https://doi.org/10.24272/j.issn.2095-8137.2022.266

Ma L, Yang JX, Lei FK, Xu MZ, Zhao YH, Jeffery WR (2023) Protection and exploration of the scientific potential of Chinese cavefish. Zoological Research 44(4): 675–677. https://doi.org/10.24272/j.issn.2095-8137.2022.484

Matzke NJ (2013) Probabilistic historical biogeography: new models for founder-event speciation, imperfect detection, and fossils allow improved accuracy and model-testing. Frontiers of Biogeography 5(4): 242–248. https://doi.org/10.21425/F55419694

Nguyen LT, Schmidt HA, Von HA, Minh BQ (2015) IQ-TREE: A fast and effective stochastic algorithm for estimating maximum-likelihood phylogenies. Molecular Biology and Evolution 32(1): 268–274. https://doi.org/10.1093/molbev/msu300

Rambaut A, Drummond AJ, Xie D, Baele G, Suchard MA (2018) Posterior summarization in Bayesian phylogenetics using Tracer 1.7. Systematic Biology 67(5): 901–904. https://doi.org/10.1093/sysbio/syy032

Ronquist F, Teslenko M, Van DMP, Ayres DL, Darling A, Höhna S, Larget B, Liu L, Suchard MA, Huelsenbeck JP (2012) MrBayes 3.2: Efficient Bayesian phylogenetic inference and model choicem across a large model space. Systematic Biology 61(3): 539–542. https://doi.org/10.1093/sysbio/sys029

Wang Y, Shen Y, Feng C, Zhao K, Song Z, Zhang Y, Yang L, He S (2016) Mitogenomic perspectives on the origin of Tibetan loaches and their adaptation to high altitude. Scientific Reports 6(1): 29690. https://doi.org/10.1038/srep29690

Wang YL (2022) Systematic taxonomy of the genus *Oreonectes* and *Troglonectes* (Master's thesis). Guizhou Normal University, Guiyang. [in Chinese]

Wen H, Luo T, Wang Y, Wang S, Liu T, Xiao N, Zhou J (2022) Molecular phylogeny and historical biogeography of the cave fish genus *Sinocyclocheilus* (Cypriniformes: Cyprinidae) in southwest China. Integrative Zoology 17(2): 311−325. https://doi.org/10.1111/1749-4877.12624

Wu F, Fang X, Yang Y, Dupont-Nivet G, Nie J, Fluteau F, Zhang T, Han W (2022) Reorganization of Asian climate in relation to Tibetan Plateau uplift. Nature Reviews Earth & Environment 3(10): 684−700. https://doi.org/10.1038/s43017-022-00331-7

Xu C, Luo T, Zhou JJ, Wu L, Zhao XR, Yang HF, Xiao N, Zhou J (2023) *Sinocyclocheilus longicornus* (Cypriniformes, Cyprinidae), a new species of microphthalmic hypogean fish from Guizhou, Southwest China. ZooKeys 1141: 1–28. https://doi.org/10.3897/zookeys.1141.91501

Yu J, Luo T, Lan C-T, Zhou J-J, Deng H-Q, Xiao N, Zhou J (2023) *Oreonectes damingshanensis* (Cypriniformes, Nemacheilidae), a new species of stream fish from Guangxi, Southwest China. ZooKeys 1180: 81–104. https://doi.org/10.3897/zookeys.1180.104645

Zhang D, Gao F, Jakovlić I, Zou H, Zhang J, Li WX, Wang GT (2020) PhyloSuite: An integrated and scalable desktop platform for streamlined molecular sequence data management and evolutionary phylogenetics studies. Molecular Ecology Resources 20(1): 348–355. https://doi.org/10.1111/1755-0998.13096

Zhang Z, Daly JS, Tian Y, Lei C, Sun X, Badenszki E, Qin Y, Hu J (2023) Late Oligocene formation of the Pearl River triggered by the opening of the South China Sea. Geophysical Research Letters 50(8): e2023GL103049. https://doi.org/10.1029/2023GL103049

Zhao X, Lan C, Luo T, Yu J, Zhou J, Xiao N, Zhou J (2024) *Karstsinnectes cehengensis* (Cypriniformes: Nemacheilidae), a new species of cave fish from Guizhou, China. Zoological Systematics 49(2): 101–115. https://doi.org/10.11865/zs.2024204

Zheng BS (1981) Freshwater fishes of Guangxi Province. Nanning: Guangxi People's Publishers, 162–163. [in Chinese]

Zhu SQ (1989) The loaches of the subfamily Nemacheilinae in China (Cypriniformes: Cobitidae). Nanjing: Jiangsu Science and Technology Publishing House, 10–25. [in Chinese]

Zhu Y, Zhu DG (2014) Description of a new species of the genus *Heminoemacheilus* (Teleostei: Balitoridae) in Guangxi, China. Journal of Guangdong Ocean University 34(6): 18–21.

Supplementary material 1

Phylogenetic tree based on mitochondrial genomes

Authors: Tao Luo, Fang-Wei Luo, Chang-Ting Lan, Ming-Yuan Xiao, Jia-Jun Zhou, Mei Liao, Ning Xiao, Jiang Zhou

Data type: png

Explanation note: In this phylogenetic tree, Bayesian posterior probabilities (BPP) from BI analyses/ultrafast bootstrap supports (UFB) from maximum likelihood analyses were noted beside nodes. The scale bar represents 0.05 nucleotide substitutions per site.

Copyright notice: This dataset is made available under the Open Database License (http://opendatacommons.org/licenses/odbl/1.0/). The Open Database License (ODbL) is a license agreement intended to allow users to freely share, modify, and use this Dataset while maintaining this same freedom for others, provided that the original source and author(s) are credited.

Link: https://doi.org/10.3897/zse.100.133964.suppl1

Supplementary material 2

Raw details of reconstruction of the ancestral area of *Karstsinnectes* at the species level using the R package BioGeoBEARS (DEC+J model)

Authors: Tao Luo, Fang-Wei Luo, Chang-Ting Lan, Ming-Yuan Xiao, Jia-Jun Zhou, Mei Liao, Ning Xiao, Jiang Zhou

Data type: png

Explanation note: The pie chart shows the probability of the most likely distribution.

Copyright notice: This dataset is made available under the Open Database License (http://opendatacommons.org/licenses/odbl/1.0/). The Open Database License (ODbL) is a license agreement intended to allow users to freely share, modify, and use this Dataset while maintaining this same freedom for others, provided that the original source and author(s) are credited.

Link: https://doi.org/10.3897/zse.100.133964.suppl2

Supplementary material 3

Raw details of reconstruction of the ancestral area of *Karstsinnectes* level using the R package BioGeoBEARS (DEC+J model)

Authors: Tao Luo, Fang-Wei Luo, Chang-Ting Lan, Ming-Yuan Xiao, Jia-Jun Zhou, Mei Liao, Ning Xiao, Jiang Zhou

Data type: png

Explanation note: The rectangular box shows the most likely distribution.

Copyright notice: This dataset is made available under the Open Database License (http://opendatacommons.org/licenses/odbl/1.0/). The Open Database License (ODbL) is a license agreement intended to allow users to freely share, modify, and use this Dataset while maintaining this same freedom for others, provided that the original source and author(s) are credited.

Link: https://doi.org/10.3897/zse.100.133964.suppl3

Supplementary material 4

Raw details of reconstruction of the ancestral area of *Karstsinnectes* at the species level using the R package BioGeoBEARS (BAYAREALIKE+J model)

Authors: Tao Luo, Fang-Wei Luo, Chang-Ting Lan, Ming-Yuan Xiao, Jia-Jun Zhou, Mei Liao, Ning Xiao, Jiang Zhou

Data type: png

Explanation note: The pie chart shows the probability of the most likely distribution.

Copyright notice: This dataset is made available under the Open Database License (http://opendatacommons.org/licenses/odbl/1.0/). The Open Database License (ODbL) is a license agreement intended to allow users to freely share, modify, and use this Dataset while maintaining this same freedom for others, provided that the original source and author(s) are credited.

Link: https://doi.org/10.3897/zse.100.133964.suppl4

Supplementary material 5

Raw measurement data used for morphological analysis

Authors: Tao Luo, Fang-Wei Luo, Chang-Ting Lan, Ming-Yuan Xiao, Jia-Jun Zhou, Mei Liao, Ning Xiao, Jiang Zhou

Data type: docx

Copyright notice: This dataset is made available under the Open Database License (http://opendatacommons.org/licenses/odbl/1.0/). The Open Database License (ODbL) is a license agreement intended to allow users to freely share, modify, and use this Dataset while maintaining this same freedom for others, provided that the original source and author(s) are credited.

Link: https://doi.org/10.3897/zse.100.133964.suppl5